POLITECNICO DI TORINO
Repository ISTITUZIONALE

Nano-metering of Solvated Biomolecules Or Nanoparticles from Water Self-Diffusivity in Bio-inspired Nanopores

Original
Nano-metering of Solvated Biomolecules Or Nanoparticles from Water Self-Diffusivity in Bio-inspired Nanopores / Bergamasco, L., Alberghini, M., Fasano, M.. - In: NANOSCALE RESEARCH LETTERS. - ISSN 1931-7573. - ELETTRONICO. - 14:1(2019), p. 336. [10.1186/s11671-019-3178-5]

Availability:
This version is available at: 11583/2765272 since: 2019-11-05T12:04:13Z

Publisher:
Springer New York LLC

Published
DOI:10.1186/s11671-019-3178-5

Terms of use:

This article is made available under terms and conditions as specified in the corresponding bibliographic description in the repository

Publisher copyright

(Article begins on next page)

09 November 2026

Nanoscale Research Letters

NANO IDEA Open Access

Nano-metering of Solvated Biomolecules Or Nanoparticles from Water Self-Diffusivity in Bio-inspired Nanopores

Luca Bergamasco[1], Matteo Alberghini[1,2] and Matteo Fasano[1*]

Abstract

Taking inspiration from the structure of diatom algae frustules and motivated by the need for new detecting strategies for emerging nanopollutants in water, we analyze the potential of nanoporous silica tablets as metering devices for the concentration of biomolecules or nanoparticles in water. The concept relies on the different diffusion behavior that water molecules exhibit in bulk and nanoconfined conditions, e.g., in nanopores. In this latter situation, the self-diffusion coefficient of water reduces according to the geometry and surface properties of the pore and to the concentration of suspended biomolecules or nanoparticles in the pore, as extensively demonstrated in a previous study. Thus, for a given pore-liquid system, the self-diffusivity of water in nanopores filled with biomolecules or nanoparticles provides an indirect measure of their concentration. Using molecular dynamics and previous results from the literature, we demonstrate the correlation between the self-diffusion coefficient of water in silica nanopores and the concentration of proteins or nanoparticles contained therein. Finally, we estimate the time required for the nanoparticles to fill the nanopores, in order to assess the practical feasibility of the overall nano-metering protocol. Results show that the proposed approach may represent an alternative method for assessing the concentration of some classes of nanopollutants or biomolecules in water.

Keywords: Water quality, Emerging pollutants, Biomolecule detection, Molecular sieves, Molecular meters, Self-diffusivity

Background

The need for water quality monitoring techniques has antique origins [1]. In ancient Rome, water sources got frequently contaminated by biological pollutants from dead bodies of men and animals or wastewater from baths, and by non-biological pollutants such as lead [2], causing severe diseases and mental problems. Continuous research and progresses across the centuries allow today most of the world population to have access to safely drinkable tap water; yet, still more than 850 million people lack primary access to clean water [3].

Accurate quality monitoring represents a challenging task, due to the different nature of the pollutants that can contaminate water, often in low concentrations. In particular, a significant number of emerging pollutants at trace levels, e.g., pharmaceuticals, chemicals, or nanomaterials, are not commonly monitored and removed by existing water treatment plants [4], although they may have adverse effects on the environment and on human health [5].

In the last decades, the advent of nanotechnologies enabled the design of tailored molecular sensors to detect different pollutants in water, such as pathogens, organic, and inorganic chemicals [6]. In their most basic version, these sensors consist of a nanostructured material, a parsing element for recognition, and an active mechanism to pass the acquired information [7]. If no quantitative information is acquired, these systems are rather referred to as nanoprobes [8] and also rely on a functionalized material to selectively detect chemicals.

In the biomedical field, the detection of biomolecules at low concentration is crucial to improve the accuracy of diagnostics and to tailor medical treatments and drugs

*Correspondence: matteo.fasano@polito.it
[1]Department of Energy, Politecnico di Torino, Corso Duca degli Abruzzi 24, 10129 Torino, Italy
Full list of author information is available at the end of the article

Springer Open

© The Author(s). 2019 **Open Access** This article is distributed under the terms of the Creative Commons Attribution 4.0 International License (http://creativecommons.org/licenses/by/4.0/), which permits unrestricted use, distribution, and reproduction in any medium, provided you give appropriate credit to the original author(s) and the source, provide a link to the Creative Commons license, and indicate if changes were made.

on the needs of the patients. Ultrasensitive identification methods have been developed to this purpose, relying on a broad variety of physical and chemical phenomena, to amplify the detection signal of low-concentrated biomolecules [9–11].

In this framework, nanoporous materials have received great attention, owing to their peculiar structure, characterized by voids and channels, which makes them particularly suitable for a number of nanotechnological applications, such as catalysis [12], adsorption heat storage [13], molecular sieving [14], selective transport (membranes) [15], nanomotion [16], drug delivery [17], and biosorption [18].

Nature has greatly inspired the development of these applications, as it provides eminent examples of efficient hierarchically porous structures with specific functionalities [19, 20]. In silico optimization and properly designed synthesis allow then to overcome possible limitations, such as low stability and little resistance to harsh environments for the required applications [21, 22].

Taking inspiration from the exoskeleton (frustule) of diatom algae [23], in this work, we conceptualize nanoporous metering tablets for the concentration of some classes of biomolecules and nanoparticles in water. The key idea is to rely on the different self-diffusion coefficient that water molecules show in bulk and nanoconfined conditions, e.g., in silica nanopores. When nanoconfined indeed, water molecules have decreased mobility and thus reduced room for diffusion. The presence of a molecular solute, e.g., nanoparticles or biomolecules, further reduces the mobility depending on its size and nature, besides the size and geometry of the pore. This behavior can be accurately recovered by a scaling law previously introduced in the literature [24], therefore demonstrating that the self-diffusion coefficient of water in a nanopore allows to indirectly quantify the concentration of biomolecules or nanoparticles contained therein. Results obtained via molecular dynamics for different concentrations of proteins and iron-oxide nanoparticles in silica nanopores show that the proposed concept yields clear insight on their concentration with satisfying accuracy.

Presentation of the Hypothesis

Bio-inspired Nano-metering Concept

Diatoms are unicellular micro-organisms (eukaryotic algae) living in ubiquitous aqueous environments. Their cells are divided in two halves, enclosed in a silicon di-oxide shell (frustule). This porous matrix (exoskeleton) allows the living cells to interact with the external environment, optimizing the attachment of nanoparticles and active bio-molecules via the hydrophilic surface and high surface-to-volume ratio [23]. The nanopores and slits of the porous matrix, along with its chemical properties, can be used for the bioinspired design of a number of nanotechnological devices for different applications [25].

Based on the structure of diatom algae, here we conceptualize nano-metering silica tablets for some classes of nanoparticles and biomolecules in water. Figure 1a shows a scanning electron microscopy of the centric diatom *Thalassiosira pseudonana* [26]. The valve consists of a porous structure characterized by channels, whose diameter ranges in the order of few nanometers, specifically around 10 nm for this case (see a detailed view in the inset). One such regular porous structure represents a natural sieve for molecules larger than the pore size,

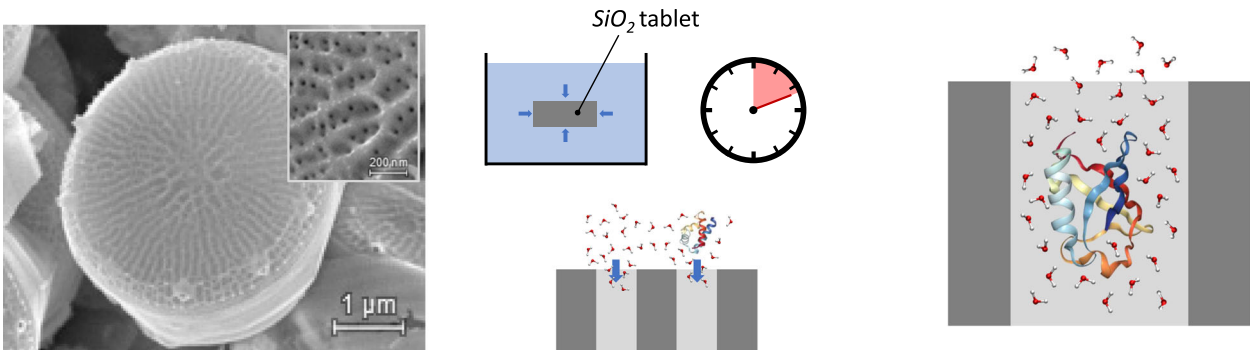

Fig. 1 Bio-inspired conceptualization of the nano-metering silica tablets. **a** Scanning electron microscopy of *Thalassiosira pseudonana*, showing the whole valve and the detail of the porous nanochannels in the insert. Image adapted from [26] and used under CC BY 4.0 license. **b** Starting from nanopores initially empty, the water molecules and solvated proteins tend to intrude into the silica nanotablets with a characteristic filling time. **c** Detail of the intrusion of ubiquitin (1UBQ) in a silica nanopore, resulting in reduced mobility of the water molecules due to the electrostatic interactions with the protein and nanopore surfaces

yet it allows intrusion of smaller molecules, providing a confining environment that can be exploited for our nano-metering concept.

If the diatom porous structure, or a similar one obtained via artificial synthesis [27], is immersed in a water sample with suspended pollutants, these latter are driven by capillarity and concentration gradient into the porous channels, see Fig. 1b, until equilibrium is reached. Inside the nanopores, water molecules have reduced mobility due to the nanoconfinement provided by the surface of the pore and intruded nanoparticles. As a consequence, the self-diffusion coefficient of water in the nanopore reduces with respect to that of the bulk, see Fig. 1c. The knowledge of this latter self-diffusion coefficient in the nanopore, which can be obtained, for example, via diffusion magnetic resonance imaging (D-MRI) [28, 29] or quasi-elastic neutron scattering (QENS) techniques [30, 31], allows to infer the concentration of the pollutants via the procedure explained in the next section.

Particle Concentration from Water Self-Diffusivity

In the proximity of solid surfaces, water molecules are subject to the effect of van der Waals and Coulomb interactions; thus, they show different behavior with respect to bulk conditions [32, 33]. In particular, those solid-liquid interactions induce a layering of the water molecules close to the solid surface, which reduces their mobility and thus the self-diffusion coefficient with respect to bulk condition.

A scaling law for predicting the self-diffusion coefficient of water that encompasses this effect has been proposed in the form [24]

$$D = D_B \left[1 + \left(\frac{D_C}{D_B} - 1 \right) \theta \right], \tag{1}$$

where D_B and D_C are the self-diffusion coefficients of water in bulk and fully nanoconfined conditions, respectively. In Eq. (1), θ is a scaling parameter that is influenced by the geometry and chemical characteristics of the solid surface, being the ratio between the nanoconfined and total water volumes in the considered configuration, namely $\theta = V_c/V_{tot}$. In particular, given a certain configuration where water is nanoconfined, V_c represents the volume of water whose mobility is significantly altered by the solid-liquid interactions, and V_{tot} the total volume accessible by water. The nanoconfined water volume V_c can be defined as the sum of the ith solvent accessible surfaces SAS_i in the given system times an average characteristic distance $\bar{\delta}_i$ below which the water molecules are significantly affected by the potential well generated by the ith solid surface, namely:

$$V_c = \sum_{i=1}^{N} \mathrm{SAS}_i \, \bar{\delta}_i \,, \tag{2}$$

being N the number of different solid-liquid interfaces in the system. The average characteristic length of water nanoconfinement exerted by a certain solid surface $\bar{\delta}_i$ can be easily estimated from atomistic simulations, once the geometrical and chemical characteristics of the surface are known [24, 34]. Note that, partial overlap of the nanoconfined water volumes may occur if several solid-liquid interfaces are present, e.g., in case of a nanopore filled with nanoparticles. In this case, the scaling parameter θ in Eq. (1) is only apparent and may take values larger than 1, thus overestimating the actual fraction of nanoconfined water. This effect can be taken into account by continuum percolation theory (CPT) [35], which provides the effective volume fraction as [24]

$$\theta^* = 1 - \exp(-\theta). \tag{3}$$

Hence, a more accurate estimation of water nanoconfinement in case of large overlaps between confining volumes can be obtained by θ^*, which, therefore, should be better employed in Eq. (1) instead of θ. Clearly, $\theta^* \approx \theta$ for $\theta \to 0$.

If the solvent accessible surface of a solvated nanoparticle (or biomolecule) is equal to SAS_i, Eq. (2) can be used to obtain the mean nanoconfined water volume per each nanoparticle (or biomolecule) as $V_{c_i} = SAS_i \, \bar{\delta}_i$. This straightforwardly yields the number of suspended nanoparticles as $n_i = V_c/V_{c_i}$ and, thus, their number concentration. Eventually, the concentration in terms of mass can be obtained via the molar mass of the considered species.

Equation 1 has been first obtained from atomistic simulations and validated against Magnetic Resonance Imaging (MRI) experiments [24]; successively, it has been validated also by QENS measures [30, 31] and applied to interpret different properties of water at solid-liquid interfaces [32, 36].

Molecular Dynamics

Simulations are carried out to demonstrate the effectiveness of Eq. (1) to infer the nanoparticle or biomolecule concentration in a hydrated nanopore, given the self-diffusion coefficient of water therein. The open-source software GROMACS [37] is employed for the molecular dynamics (MD) simulations. To analyze the different mobility of water in bulk and nanoconfined conditions, two different geometric layouts are analyzed. For bulk conditions, a cubic computational box is adopted, where periodicity is applied along the three Cartesian axes. For nanoconfined conditions, a simplified representation of the pore in the nano-metering silica tablets is adopted, consisting of a single cylindrical nanopore (see Fig. 1c). For the sake of simplicity, but without loss of generality, a regular pore shape/size distribution is assumed, and thus, periodicity is applied along the axes.

The geometry files for the considered proteins (ubiquitin - 1UBQ; hen egg-white lysozyme - 1AKI) were obtained from the Protein Data Bank [38] database, whereas both the silica nanopores and magnetite nanoparticles were available from a previous study [24]. The intra-molecular bonded interactions in the silica nanopores and iron oxide nanoparticles are modeled by harmonic stretching and angle potentials, as detailed in [24]. Their non-bonded interactions are modeled by 12-6 Lennard-Jones and electrostatic potentials, as also reported in [24]. Bonded and non-bonded interactions of the proteins are taken from GROMOS96 43a2 [39]. Notice that, during the equilibration, all bonds in the proteins are kept rigid using the LINCS (Linear Constraint Solver) algorithm [40]. The SPC/E water model [41] with rigid bonded interactions is adopted in all cases, as it accurately recovers the most relevant properties of water at room temperature [42].

In both bulk and nanoconfined configurations, the system is first energy minimized, solvated (water density approximately equal to 1.00 g/cm^3) and, for proteins, the net charge neutralized via ion addition. In detail, chloride ions are introduced in the simulation box to neutralize the net positive charge of lysozyme, whereas ubiquitin is neutral and thus does not require any ion addition. Next, the hydrated system is relaxed to its energy minimum for a sufficient time. The temperature of the system is then equilibrated by a simulation in the NVT ensemble for 100 ps (T = 300 K, Nosé-Hoover thermostat) to achieve convergence of potential energy in the simulated configuration (about ± 1% fluctuations around the equilibrium value, see Additional file 1: Figure S1c). After that, bulk configurations are also equilibrated in the NPT ensemble for 100 ps (T = 300 K, Nosé-Hoover thermostat; p = 1 bar, Parrinello-Rahman barostat) to achieve convergence of water density in the simulated setups (about ± 2% fluctuations around the equilibrium value, see Additional file 1: Figure S1a). The production run is finally performed in the NVT ensemble (T = 300 K, Nosé-Hoover thermostat). In all simulated cases, steady state is considered as reached when the self-diffusion coefficient, which is evaluated every 100 ps, tends to an asymptotic value (i.e., ± 10% fluctuations around the moving average, see Additional file 1: Figure S1b and d). Since this is generally achieved after ≈ 500 ps for the bulk configurations or ≈ 1000 ps for the nanoconfined ones, the former are continued up to 1 ns, the latter up to 2 ns to have better statistics. In all runs, the leap-frog algorithm with time step 0.001 ps is used, while a 1.2-nm cut-off distance is adopted for the van der Waals interactions and a Particle Mesh Ewald (PME) method for the electrostatic ones (mesh spacing 0.16 nm). The solvent accessible surface of the solid nano-objects is obtained from the production run and fed into a dedicated routine (see the Supplementary software in [24]), which, based on the adopted force field, computes the average characteristic length of nanoconfinement $\bar{\delta}_i$ per each ith solid-liquid interface in the setup.

Testing the Hypothesis

Water Self-Diffusion for Different Systems

The validity of the scaling law in Eq. (1) has been first tested considering both results from the literature (14 configurations) and new simulations (9 configurations). In particular, the configurations taken from the literature are hydrated silica nanopores with diameter d_P = 8.13 or 11.04 nm (see Supplementary Table S1 in [24]); sole magnetite nanoparticles with diameter d_p = 1.27 or 1.97 nm immersed in cubic water boxes with 6 or 7 nm side, respectively (see Supplementary Table S4 in [24]); sole 1AKI or 1UBQ proteins immersed in cubic water boxes with 7.03 or 6.32 nm side, respectively (see Supplementary Table S10 in [24]); a hydrated silica nanopore with diameter d_P = 8.13 nm filled with 2, 4, 8, or 16 magnetite nanoparticles with diameter d_p = 1.97 nm (see Supplementary Table S2 in [24]) or 16 magnetite nanoparticles with diameter d_p = 1.27 nm (see Supplementary Table S3 in [24]); and a hydrated silica nanopore with diameter d_P = 11.04 nm filled with 36 or 66 magnetite nanoparticles with diameter d_p = 1.27 nm or 20 magnetite nanoparticles with diameter d_p = 1.97 nm (see Supplementary Table S3 in [24]). Furthermore, the new simulated setups are a hydrated silica nanopore with diameter d_P = 8.13 nm filled with one 1UBQ protein and a hydrated silica nanopore with diameter d_P = 11.04 nm filled with 2, 3 or 9 1AKI proteins, or 2, 7, 9 or 12 1UBQ proteins.

Figure 2 shows the scaling behavior for the self-diffusion coefficient of water for the different systems previously listed, namely bulk water (D_B = 2.60 × 10^{-9} m^2/s), hydrated silica nanopores, solvated proteins and magnetite nanoparticles, and hydrated silica nanopores filled with proteins or nanoparticles. As expected, water inside the silica nanopores shows reduced self-diffusion, coherently with the increasing degree of nanoconfinement represented by the scaling parameter θ^*. Suspended molecules (nanoparticles and proteins) show a similar effect on the self-diffusion coefficient of water. In Fig. 2, the solid line corresponds to Eq. (1) with $D_C/D_B \approx 0$, which represents the limiting case of assuming that nanoconfined water molecules have no mobility and are therefore unable to diffuse. The dashed line corresponds, instead, to the same equation with a more realistic value of $D_C = 0.39 \times 10^{-9}$ m^2/s, as observed in the simulations reported in [24]: this model is able to accurately recover the simulation results (R^2= 0.93), therefore confirming the good prediction capabilities of Eq. (1) also for the new simulated configurations.

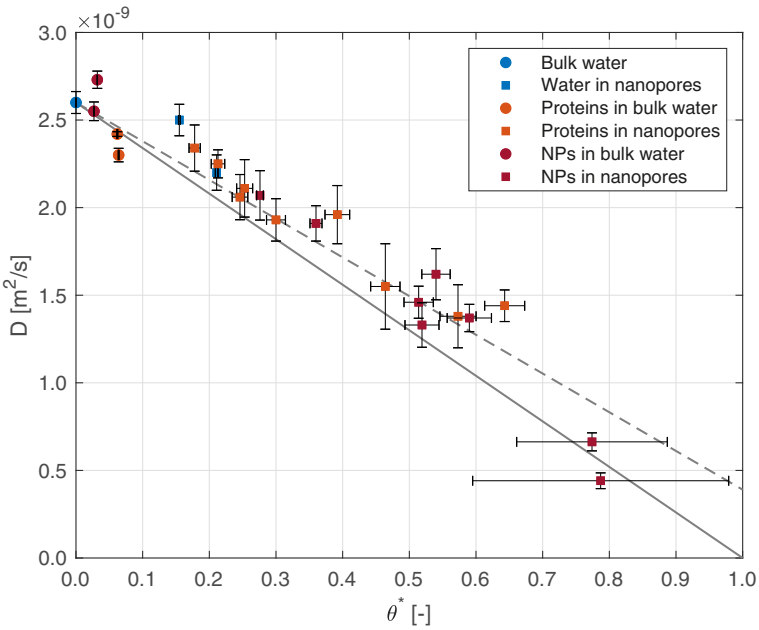

Fig. 2 Water self-diffusion coefficient for different systems. The self-diffusion coefficient of water is shown against the scaling parameter θ^* for different systems. Data for proteins in silica nanopores have been obtained via molecular dynamics, while the rest of the data from the Supplementary information in [24]. In the legend, nanoparticles are abbreviated as NPs. The uncertainties on the value of D refer to the fitting of the mean square displacement (±1 s.d.); the uncertainties on the value of θ^* to the estimate of the total volume accessible to water molecules (±1 s.d.). The solid and dashed lines report the model in Eq. (1) in case of $D_C = 0$ and $D_C = 0.39 \times 10^{-9}$ m^2/s, respectively

Examples of the Proposed Protocol in Practice

Let us consider a nanoporous silica tablet used as metering device for a known polluting agent in water, as proposed. Let us assume that the tablet is left immersed in a solution test sample for sufficient time so that the suspended polluting molecules diffuse into the tablet and equilibrium is reached (see the next section for a detailed discussion on this). The sample is then extracted and the self-diffusion coefficient of water D inside the porous structure of the tablet obtained by, e.g., QENS measure. The volume fraction θ^* can be then easily obtained from Eq. (1), since both D_B and D_C are known at a given temperature. Then, the overlapped nanoconfined volumes of water can be taken into account by CPT, thus leading to $\theta = -\ln(1-\theta^*)$. For a single type of polluting agent enclosed in one nanopore, Eq. (2) simplifies to

$$V_c = n_p \mathrm{SAS}_p \bar{\delta}_p + \mathrm{SAS}_P \bar{\delta}_P , \tag{4}$$

being the subscripts p and P referred to the particles and pore, respectively. Once the solvent accessible area SAS and the mean characteristic length of nanoconfinement $\bar{\delta}$ for particles and pores are known from molecular dynamics, the number of suspended particles is easily obtained as

$$n_p = \frac{V_{\mathrm{tot}}\theta - \mathrm{SAS}_P\bar{\delta}_P}{\mathrm{SAS}_p\bar{\delta}_p}. \tag{5}$$

The results of this nano-metering procedure are reported in Tab. 1 and Fig. 3, for some sample cases of proteins and nanoparticles inside silica nanopores from Fig. 2. In particular, the bisector curve in Fig. 3 allows to appreciate the accuracy of the estimated number of suspended particles (n_p^e) with respect to the original (actual) one (n_p^o), being the R^2 of the curve equal to 0.85.

Given the number of biomolecules or nanoparticles in the nanopore, their number concentration can be readily obtained as $c = n_p/V_\mathrm{P}$, being $V_\mathrm{P} = T\pi d_P^2/4$ the free volume of the pore in case of a cylindrical through configuration [27] (T is the pore length, that is, e.g., the thickness of the silica tablet in case of straight pores). This nano-metering protocol has been here presented for a single pore, but it could be easily extrapolated to the whole nano-metering tablet given its porosity and thus number of hydrated nanopores.

Filling of the Nanopores

The examples discussed in the previous section account for equilibrium conditions, thus assuming that the concentration of particles in the nanopore equals that in the bulk solution. Nevertheless, the nano-metering protocol suggested in this work would also involve the filling process of nanopores by the solvated particles to be detected. In this section, we assess the practical feasibility of the

Table 1 Data employed for demonstrating the effectiveness of the proposed nano-metering protocol

MOL	d_P [nm]	d_p [nm]	n_p^o	D [m^2/s]	θ^*	θ	V_{tot} [nm^3]	δ_p [nm]	SAS$_p$ [nm^2]	δ_P [nm]	SAS$_p$ [nm^2]	n_p^e
IONP	8.13	1.97	4	1.91E−09	0.31	0.37	200.75	0.50	21.64	0.33	140.47	2.66
IONP	8.13	1.97	8	1.33E−09	0.57	0.85	180.90	0.50	21.64	0.33	140.47	10.06
IONP	8.13	1.27	16	1.46E−09	0.52	0.73	193.59	0.46	12.61	0.33	140.47	16.16
IONP	11.04	1.27	36	1.62E−09	0.44	0.59	351.63	0.46	12.61	0.33	194.00	24.47
IONP	11.04	1.97	20	1.37E−09	0.56	0.81	313.15	0.50	21.64	0.33	194.00	17.74
IONP	11.04	1.27	66	6.63E−10	0.88	2.09	300.98	0.46	12.61	0.33	194.00	97.30
1AKI	11.04	–	2	2.06E−09	0.24	0.28	375.71	0.32	67.36	0.33	194.00	1.95
1AKI	11.04	–	3	1.93E−09	0.30	0.36	357.35	0.32	67.36	0.33	194.00	3.08
1AKI	11.04	–	9	1.44E−09	0.52	0.74	247.23	0.32	67.36	0.33	194.00	5.66
1UBQ	11.04	–	7	1.96E−09	0.29	0.34	338.10	0.31	48.19	0.33	194.00	3.48
1UBQ	11.04	–	9	1.55E−09	0.47	0.64	316.87	0.31	48.19	0.33	194.00	9.38
1UBQ	11.04	–	12	1.38E−09	0.55	0.81	285.02	0.31	48.19	0.33	194.00	11.14

Data for the iron-oxide nanoparticles (IONP) have been taken from the supplementary information in [24], while those for proteins (1AKI and 1UBQ) have been computed for the present work. Notice that Eq. (1) has been applied considering $D_C = 0.39 \times 10^{-9}$ m^2/s. n_p^e is the number of particles estimated using the proposed protocol; n_p^o the original (actual) number of particles in the simulated setups

suggested nano-metering protocol with respect to the characteristic filling time of the nanopores.

The experimental protocol commonly used to maximize the filling of nanopores by solvated nanoparticles includes sonication and centrifugation processes [43], which in some cases may lead to a non-uniform distribution of particles due to cluster creation and clogging of the nanochannels [44–47]. Here, we consider a spontaneous solvent imbibition and diffusion of the dispersed particles into the initially dry nanopores. Hence, we adopt a simplified approach, considering two successive processes because of the very different time scales of the involved phenomena: capillary imbibition of the dry pores by the pure fluid, and particle diffusion by Fickian mechanism through the hydrated pores to equilibrium conditions.

Experiments and molecular dynamic simulations [48–50] show that if the average capillary diameter is greater than approximately four times the molecular diameter of water [50, 51], the imbibition process can be

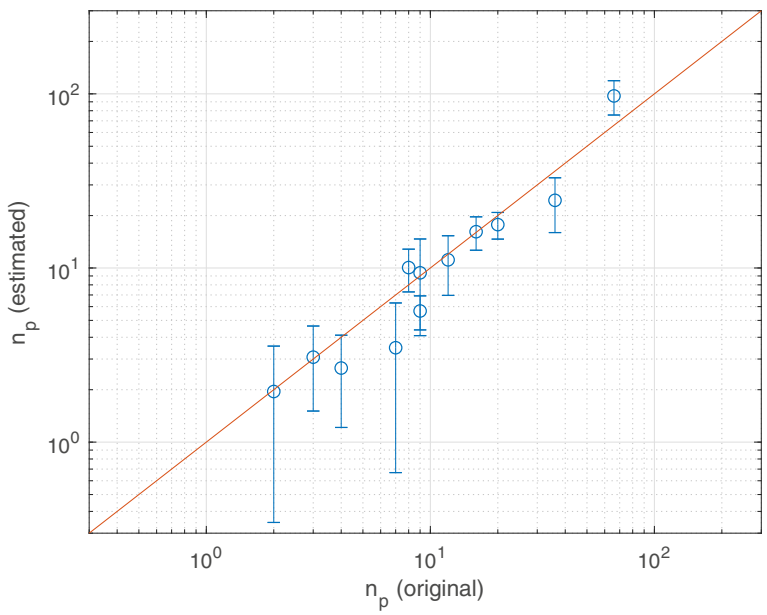

Fig. 3 Accuracy of the proposed nano-metering protocol. Estimated number of particles using the proposed protocol vs the original number of particles. The reported data (dots) refer to the configurations in Table 1; the solid line is the bisector. The error bars on the value of n_p^e are computed from the variability of D and V_{tot} values (uncertainty quantification, ± 1 s.d.)

described by the Lucas-Washburn (LW) equation. Under the sharp-front approximation, Darcy's law can be used to model the position of the moving front $h(t)$, recovering the same form of the LW equation [52]:

$$h = \sqrt{\frac{2K\Delta p}{\phi_i \mu} t}, \tag{6}$$

where Δp is the driving capillary pressure, μ is the dynamic viscosity of the fluid (water in this case), ϕ_i is the effective porosity of the medium at the beginning of the uptake process, and K is its permeability. Porous silica materials present a very regular structure and a narrow pore size distribution [46]; thus, their permeability can be computed as [49, 53]:

$$K = \frac{1}{8} \frac{r_h^4 \phi_0}{r_0^2 \tau}, \tag{7}$$

where r_0 is the nominal pore diameter, r_h is the hydraulic diameter of the pore (smaller than r_0 because of the adsorbed layer of water molecules on the capillary surface), ϕ_0 is the nominal porosity of the medium, and τ is its tortuosity. The capillary pressure can be described by the Young-Laplace equation:

$$\Delta p = \frac{2\sigma \cos(\vartheta)}{r_h}, \tag{8}$$

where σ is the surface tension of the fluid and ϑ its dynamic contact angle with respect to the pore surface. Note that, for silica-water interfaces, $\vartheta \approx 0$ [49, 54].

Nanoporous tablets can be precisely manufactured with straight cylindrical pores ranging from 5 to 150-nm diameter and porosity from 40 to 90% [27]. Equation 6 can be employed to estimate the time required for the complete imbibition of a nanoporous material with such geometrical characteristics (t_i), in the simplifying hypothesis that diluted contaminants do not affect this process. The resulting t_i are reported in Fig. 4 using blue asterisks and dotted line, for tablet thickness (i.e., pore length) varying from 1 μm to 1 mm. The results show a remarkable speed of the imbibition process: the thickest macroscopic tablet considered is completely filled with water in less than 10 s. In order to analyze coherent configurations with those simulated by molecular dynamics setups, the estimates of t_i consider an initially dry material (i.e., $\phi_0 = \phi_i$), an average pore diameter of $d_0 = 2r_0 = 11.04$ nm, porosity and tortuosity equal to $\phi_0 \approx 40\%$ and $\tau \approx 1$, respectively. Since the hydrodynamic radius should take into account the effect of adsorbed water molecules, $r_h = r_0 - 2d_w$, where two layers of adsorbed water molecules (with $d_w = 0.275$-nm diameter) are assumed [24]. The remaining water within the pores can be reasonably considered at bulk conditions, and thus, $\sigma = 0.072$ N/m and $\mu = 10^{-3}$ Pa·s at $T = 300$ K. These estimates are performed neglecting the effect of the suspended particles on the imbibition process. However, particle-wall interactions are not negligible at high volume fractions or for particle-pore size ratios close to unit, as local properties of water such as viscosity and contact angle may be altered [55]. Still, the position of the liquid front can be described by Eq. (6) for particle-pore size ratios of 10% or lower [55].

The characteristic time required for particle diffusion into the fully hydrated, homogeneous, and straight nanopores is then assessed. This filling process is assumed to rely on pure diffusion [56, 57] and, under the assumption of negligible particle-pore interactions, can be described by Fick's equation:

$$\phi_0 \frac{\partial c_i}{\partial t} - D_e \nabla^2 c_i = 0, \tag{9}$$

being c_i the particle concentration, $D_e = \phi_0 D_p / \tau$ the effective diffusivity of the particles in the hydrated channels, and D_p their diffusivity in the bulk fluid.

Computations are performed, as a first example, considering a diluted lysozyme (1AKI) solution at $c_{i,b} = 3.4$ mol/m^3 concentration, i.e., approximately 1% weight fraction. Similarly to the configuration employed to estimate t_i, silica tablets with an average pore diameter of $d_0 = 2r_0 = 11.04$ nm, varying thickness, porosity equal to $\phi_0 \approx 40\%$, and tortuosity $\tau \approx 1$ are considered. Starting from a fully hydrated pore without any particle inside, the filling time t_D is estimated as the time required to reach $c_{i,c} = 0.95 c_{i,b}$ at the center of the pore, namely at $x = T/2$. The particle concentration is constant and equal to $c_{i,b}$ at both ends of the channel, namely at $x = 0$ and T. The diffusion coefficient of the lysozyme in water is assumed equal to the bulk value, namely $D_p = 11.08 \cdot 10^{-11}$ m^2/s [58, 59]. Equation 9 is solved numerically in one dimension by a finite-element method. The results are reported in Fig. 4 as red stars and dashed line, showing that t_D is about two orders of magnitude higher than t_i for a given thickness of the silica tablet. Even in the worst case presented ($T = 1$ mm, $t_D \approx 3000$ s), the filling time appears to be compatible with a nano-metering protocol of practical interest. Note that both simulations [60] and experiments [61] in the literature show that the particle diffusivity D_p in nanopores can be significantly lower than the bulk one, because of the different affinity of particles with the pore surface and the presence of nanoconfined water with low mobility. Hence, the proposed approach provides initial indications on the characteristic filling time but, to achieve more accurate estimations, D_p and thus t_D should be analyzed on a case-by-case basis [62].

As a second example, we assess the possibility of metering the concentration of solvated drugs, since they are currently considered as emerging pollutants of water sources [5]. In particular, we analyze one of the relevant drugs for cancer treatment: doxorubicin, which is a hydrophobic molecule commonly used for chemotherapy [63–65].

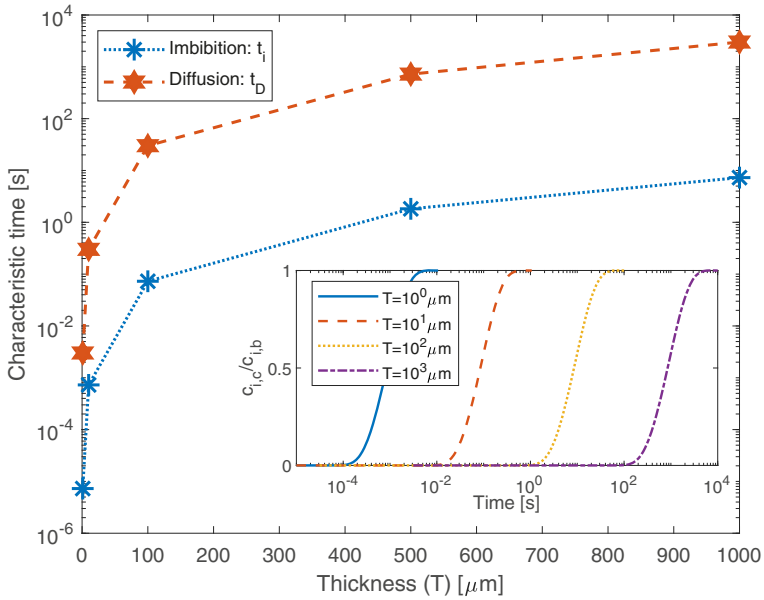

Fig. 4 Characteristic filling times of the nanopores. Characteristic times of the nanopore filling by capillarity (blue dotted line, t_i) and particle diffusion (red dashed line, t_D) varying the thickness of the nanoporous silica tablet (nanopores with 11.04-nm diameter; solution of 1AKI proteins in water at 1% weight fraction). The particle diffusion process through the fully hydrated pores requires a characteristic time t_D two orders of magnitude higher than t_i, in all the analyzed configurations. The inset shows the ratio between the particle concentration at the center of the nanopore ($c_{i,c}$, at $x = T/2$) and the bulk one ($c_{i,b}$, at $x = 0$ and T) as a function of time for different thickness (T) of the tablets

An estimation of the diffusion time t_D of doxorubicin into the hydrated silica nanotablets can be performed under the assumptions already adopted for the previous case study. Unbound doxorubicin has a diffusion coefficient of $D_p = 1.6 \cdot 10^{-10}$ m^2/s [66]; thus, a silica tablet with 500 μm thickness would be filled at 95% of the bulk concentration ($c_{i,b} = 3.4$ mol/m^3) in approximately 500 s. This illustrative case shows that the proposed nano-metering protocol could be also potentially employed to detect the concentration of drug traces in water. We remark that the effect of additional factors (e.g., chemical affinity between drugs and pore surface, pH, presence of surfactants or functionalizations), which are not considered in this simplified model, should be experimentally investigated, as they may significantly deviate the characteristic time with respect to the considered simplified conditions.

Clearly, the filling time of the nanopores should lie between t_i (best case, nanoparticles are dragged into the pores together with water by capillarity) and t_D (worst case, water first hydrates the pores and then nanoparticles follow by Fickian diffusion). Even in the worst explored case, modeling estimations of the filling time of the nanopores indicate a practical feasibility of the proposed nano-metering protocol. This idea is also supported by some promising experimental evidences in the literature. For instance, hydrophilic carbon nanotubes with average diameter of 300 nm are easily filled by spontaneous imbibition with particles in the range of 10–50 nm [67, 68], proving that a proper tuning of the geometrical and chemical parameters of the configuration would provide a fast and homogeneous filling of the nanochannels, thus making the proposed nano-metering protocol feasible.

Implications of the Hypothesis

Inspired by the regular nanoporous structure of diatom algae frustules, in this work, we have presented a new concept for measuring the concentration of nanoparticles or biomolecules dispersed in water. The regular structure of the algae frustules can be artificially reproduced by nanoporous silica tablets, whose pore size, thickness, and shape should be precisely tuned to optimize the selective uptake of particles. The proposed nano-metering method relies on the effect of those nanoparticles or biomolecules on the self-diffusion coefficient of water nanoconfined within the tablet's pores, and consists in the following steps:

1. Synthesize porous tablet with a controlled size distribution of nanopores.
2. Let the nanopores of the tablet fill with the solution containing the particles to be detected via capillary imbibition and particle diffusion, achieving equilibrium conditions between the nanopores and the surrounding solution.

3. Remove the tablet from the solution and measure the self-diffusion coefficient of water in the hydrated nanopores filled with the particles, e.g., by QENS or D-MRI techniques.
4. Correlate the measured self-diffusion coefficient of water with the particle concentration by means of Eqs. 1 to (5). The solvent accessible surface of nanopore and particles (*SAS*) and their mean characteristic length of nanoconfinement ($\bar{\delta}$) should be computed from molecular dynamics or taken from available databases.

Molecular dynamic simulations and evidence from the literature have been employed to assess the feasibility of the proposed nano-metering protocol. Hydrated nanopores filled with different concentrations of iron-oxide nanoparticles or proteins have been analyzed, finding agreement between the computed and predicted self-diffusion coefficient of nanoconfined water, thus allowing to estimate the particle concentration. A preliminary analysis of the mechanisms involved in the nanopores filling has been also carried out. Because of the different time scales, two different phenomena have been considered separately: the imbibition of a dry tablet by pure water, driven by capillarity, and the particle diffusion through the hydrated pores, driven by concentration gradient. Results show that the leading characteristic time in the filling process is the time required for particles to diffuse into the hydrated pores; however, the estimated filling time does not exceed 1 h even in case of the thickest tablets considered (1 mm), therefore not compromising the practical feasibility of the nano-metering protocol.

Although the proposed nano-metering method has shown promising results from a numerical point of view, the actual experimental implementation may have to face some additional issues. First, the interaction between the pore surface and particles could be non-negligible and thus alter the filling process (e.g., pores clogging). This effect could generate a bias between the actual concentration of the particles in the bulk solution and the one measured within the pores. Such an issue could be solved by an accurate selection of the surface properties of the pores, which should not interact with the particles to be detected. Second, the current experimental techniques could have difficulty to measure the water diffusivity with a single-nanopore resolution. This issue could be mitigated by measuring the average self-diffusion coefficient over hundreds or thousands of nanopores, which could also provide a better statistical sampling in case of inhomogeneous particle filling throughout the tablet. Third, the uncertainty of the nano-metering protocol should be assessed by experiments. The configurations studied by molecular dynamics have revealed prediction errors up to $\pm$ 50%: this error range could be eventually reduced by considering larger statistical samples, both in terms of time (multiple measures) and space (averages over hundreds or thousands of pores). Fourth, the optimal diameter of the nanopores should be determined on the basis of the expected size and concentration of the particles to be detected. On the one hand, the pore size should be chosen to avoid low θ^* (e.g., θ^* should be $>$ 0.2), since this could lead to negligible variations of the self-diffusivity of water that could be eventually below the resolution of the QENS or D-MRI techniques; on the other hand, high levels of water nanoconfinement should be avoided as well (e.g., θ^* should be $<$ 0.8), to limit the risk of pore clogging or particle aggregation/segregation and thus biased concentration results.

In conclusion, further research is needed to validate experimentally the original nano-metering protocol discussed in this work. However, the presented numerical results prove the potential of the idea, which may pave the way to a completely new class of detection processes of emerging nanopollutants in water or biomolecules. In perspective, the microscopic size of the metering devices, e.g., nanoporous silica tablets, may allow automation of the nano-metering process through lab-on-a-chip devices.

Supplementary information

Supplementary information accompanies this paper at https://doi.org/10.1186/s11671-019-3178-5.

Additional file 1: PDF file containing a multi-panel figure showing the energy, density, and self-diffusion coefficient convergence for some illustrative molecular dynamics simulations (bulk and nanoconfined setups)

Abbreviations

1AKI: Lysozyme; 1UBQ: Ubiquitin; CPT: Continuum percolation theory; D-MRI: Diffusion magnetic resonance imaging; IONP: Iron oxide nanoparticle; LINCS: Linear constraint solver; LW: Lucas-Washburn; MD: Molecular dynamics; MOL: Molecule; MRI: Magnetic resonance imaging; NP: Nanoparticle; PME: Particle Mesh Ewald; QENS: Quasi-elastic neutron scattering; SAS: Solvent accessible surface

Acknowledgements

The authors acknowledge Mr. Ruben Minoggio and Mr. Daniele Borri for helping in the setup and run of some of the reported simulations.

Authors' Contributions

MF carried out the MD simulations. LB analyzed and interpreted the MD simulation results. MA studied the filling process of the nanopores. LB and MA drafted the first version of the manuscript. MF conceived and supervised the study. All authors contributed to write the manuscript and approved it in the final form.

Funding

M.F. acknowledges financial support from Politecnico di Torino through the RTDa Starting Grant (grant number 56_RIL16FAM01).

Availability of data and materials

The datasets used and/or analyzed during the current study are available from the corresponding author on reasonable request.

Competing Interests

The authors declare that they have no competing interests.

Author details
[1]Department of Energy, Politecnico di Torino, Corso Duca degli Abruzzi 24, 10129 Torino, Italy. [2]Clean Water Center, Politecnico di Torino, Corso Duca degli Abruzzi 24, 10129 Torino, Italy.

Received: 31 July 2019 Accepted: 4 October 2019
Published online: 28 October 2019

References

1. Vitruvius (1924) De Architectura (translated by Morgan, MH). Harvard University Press, Cambridge
2. Delile H, Blichert-Toft J, Goiran J-P, Keay S, Albarède F (2014) Lead in ancient Rome's city waters. Proc Nat Acad Sci 111(18):6594–6599
3. WHO/UNICEF (2017) Progress on drinking water, sanitation, and hygiene: 2017 Update and SDG Baselines. World Health Organization (WHO) and the United Nations Children‰s Fund (UNICEF), Geneva
4. Gogoi A, Mazumder P, Tyagi VK, Chaminda GT, An AK, Kumar M (2018) Occurrence and fate of emerging contaminants in water environment: a review. Groundwater Sustain Dev 6:169–180
5. Geissen V, Mol H, Klumpp E, Umlauf G, Nadal M, van der Ploeg M, van de Zee SE, Ritsema CJ (2015) Emerging pollutants in the environment: a challenge for water resource management. Int Soil Water Conserv Res 3(1):57–65
6. Vikesland PJ (2018) Nanosensors for water quality monitoring. Nature Nanotechnol 13(8):651
7. Vikesland PJ, Wigginton KR (2010) Nanomaterial enabled biosensors for pathogen monitoring - a review. Environ Sci & Technol 44(10):3656–3669
8. Rodrigues SM, Demokritou P, Dokoozlian N, Hendren CO, Karn B, Mauter MS, Sadik OA, Safarpour M, Unrine JM, Viers J, et al (2017) Nanotechnology for sustainable food production: promising opportunities and scientific challenges. Environ Sci: Nano 4(4):767–781
9. Zhou S, Yuan L, Hua X, Xu L, Liu S (2015) Signal amplification strategies for DNA and protein detection based on polymeric nanocomposites and polymerization: A review. Anal Chim Acta 877:19–32
10. Smith SJ, Nemr CR, Kelley SO (2017) Chemistry-driven approaches for ultrasensitive nucleic acid detection. J Am Chem Soc 139(3):1020–1028
11. Xu J-J, Zhao W-W, Song S, Fan C, Chen H-Y (2014) Functional nanoprobes for ultrasensitive detection of biomolecules: an update. Chem Soc Rev 43(5):1601–1611
12. Wang N, Sun Q, Yu J (2019) Ultrasmall metal nanoparticles confined within crystalline nanoporous materials: a fascinating class of nanocatalysts. Adv Mater 31(1):1803966
13. Fasano M, Falciani G, Brancato V, Palomba V, Asinari P, Chiavazzo E, Frazzica A (2019) Atomistic modelling of water transport and adsorption mechanisms in silicoaluminophosphate for thermal energy storage. Appl Thermal Eng 160:114075
14. Fasano M, Chiavazzo E, Asinari P (2014) Water transport control in carbon nanotube arrays. Nanoscale Res Lett 9(1):559
15. Fasano M, Humplik T, Bevilacqua A, Tsapatsis M, Chiavazzo E, Wang EN, Asinari P (2016) Interplay between hydrophilicity and surface barriers on water transport in zeolite membranes. Nature Commun 7:12762
16. Fasano M, Crisafulli A, Cardellini A, Bergamasco L, Chiavazzo E, Asinari P (2019) Thermally triggered nanorocket from double-walled carbon nanotube in water. Mol Simulat 45(4-5):417–424
17. Key J, Palange AL, Gentile F, Aryal S, Stigliano C, Di Mascolo D, De Rosa E, Cho M, Lee Y, Singh J, et al (2015) Soft discoidal polymeric nanoconstructs resist macrophage uptake and enhance vascular targeting in tumors. ACS nano 9(12):11628–11641
18. Lu GQ, Zhao XS (2004) Nanoporous materials: science and engineering, Vol. 4. Imperial College Press, United Kingdom
19. Yang X-Y, Chen L-H, Li Y, Rooke JC, Sanchez C, Su B-L (2017) Hierarchically porous materials: synthesis strategies and structure design. Chem Soc Rev 46(2):481–558
20. Sanchez C, Arribart H, Guille MMG (2005) Biomimetism and bioinspiration as tools for the design of innovative materials and systems. Nature Mater 4(4):277
21. Heo J, Kang T, Jang SG, Hwang DS, Spruell JM, Killops KL, Waite JH, Hawker CJ (2012) Improved performance of protected catecholic polysiloxanes for bioinspired wet adhesion to surface oxides. J Am Chem Soc 134(49):20139–20145
22. Munch E, Launey ME, Alsem DH, Saiz E, Tomsia AP, Ritchie RO (2008) Tough, bio-inspired hybrid materials. Science 322(5907):1516–1520
23. Seckbach J, Kociolek P (2011) The Diatom World. 1st. Springer, Netherlands
24. Chiavazzo E, Fasano M, Asinari P, Decuzzi P (2014) Scaling behaviour for the water transport in nanoconfined geometries. Nature Commun 5:3565
25. Pedro Gómez-Romero CS (2004) Functional hybrid materials. 6th. John Wiley & Sons, New Jersey, USA
26. Köhler L, Machill S, Werner A, Selzer C, Kaskel S, Brunner E (2017) Are diatoms "green" aluminosilicate synthesis microreactors for future catalyst production? Molecules 22(12):2232
27. Godin B, Chiappini C, Srinivasan S, Alexander JF, Yokoi K, Ferrari M, Decuzzi P, Liu X (2012) Discoidal porous silicon particles: fabrication and biodistribution in breast cancer bearing mice. Adv Func Mater 22(20):4225–4235
28. Topgaard D (2017) Multidimensional diffusion MRI. J Magnetic Resonance 275:98–113
29. Demberg K, Laun FB, Windschuh J, Umathum R, Bachert P, Kuder TA (2017) Nuclear magnetic resonance diffusion pore imaging: experimental phase detection by double diffusion encoding. Phys Rev E 95(2):022404
30. Diallo S (2015) Pore-size dependence and characteristics of water diffusion in slit-like micropores. Phys Rev E 92(1):012312
31. Osti NC, Cote A, Mamontov E, Ramirez-Cuesta A, Wesolowski D, Diallo S (2016) Characteristic features of water dynamics in restricted geometries investigated with quasi-elastic neutron scattering. Chem Phys 465:1–8
32. Morciano M, Fasano M, Nold A, Braga C, Yatsyshin P, Sibley DN, Goddard BD, Chiavazzo E, Asinari P, Kalliadasis S (2017) Nonequilibrium molecular dynamics simulations of nanoconfined fluids at solid-liquid interfaces. J Chem Phys 146(24):244507
33. Zaragoza A, Gonzalez MA, Joly L, López-Montero I, Canales MA, Benavides AL, Valeriani C (2019) Molecular dynamics study of nanoconfined tip4p/2005 water: how confinement and temperature affect diffusion and viscosity. Phys Chem Chem Phys 21:13653–13667
34. Cardellini A, Fasano M, Chiavazzo E, Asinari P (2016) Interfacial water thickness at inorganic nanoconstructs and biomolecules: size matters. Phys Lett A 380(20):1735–1740
35. Stauffer D, Aharony A (2014) Introduction to percolation theory. 2nd. Taylor & Francis, United Kingdom
36. De Almeida JM, Miranda CR (2016) Improved oil recovery in nanopores: NanoIOR. Sci Rep 6:28128
37. Abraham MJ, Murtola T, Schulz R, Páll S, Smith JC, Hess B, Lindahl E (2015) GROMACS: high performance molecular simulations through multi-level parallelism from laptops to supercomputers. SoftwareX 1-2:19–25
38. Protein Data Bank. https://www.rcsb.org/. Accessed 14 June 2019
39. Schuler LD, Daura X, Van Gunsteren WF (2001) An improved GROMOS96 force field for aliphatic hydrocarbons in the condensed phase. J Comput Chem 22(11):1205–1218
40. Hess B, Bekker H, Berendsen HJ, Fraaije JG (1997) LINCS: a linear constraint solver for molecular simulations. J Comput Chem 18(12):1463–1472
41. Berendsen H, Grigera J, Straatsma T (1987) The missing term in effective pair potentials. J Phys Chem 91(24):6269–6271
42. van der Spoel D, van Maaren PJ, Berendsen HJ (1998) A systematic study of water models for molecular simulation: derivation of water models optimized for use with a reaction field. J Chem Phys 108(24):10220–10230
43. Hlady V, Buijs J, Jennissen HP (1999) Methods for studying protein adsorption. Methods Enzymol 309:402–429
44. Gizzatov A, Key J, Aryal S, Ananta J, Cervadoro A, Palange AL, Fasano M, Stigliano C, Zhong M, Di Mascolo D, et al (2014) Hierarchically structured magnetic nanoconstructs with enhanced relaxivity and cooperative tumor accumulation. Adv Funct Mater 24(29):4584–4594
45. Gross AF, Diehl MR, Beverly KC, Richman EK, Tolbert SH (2003) Controlling magnetic coupling between cobalt nanoparticles through nanoscale confinement in hexagonal mesoporous silica. J Phys Chem B 107(23):5475–5482
46. Deere J, Magner E, Wall J, Hodnett B (2001) Adsorption and activity of cytochrome c on mesoporous silicates. Chem Commun 5:465–465
47. Deere J, Magner E, Wall J, Hodnett B (2003) Adsorption and activity of proteins onto mesoporous silica. Catalys Lett 85(1-2):19–23
48. Dimitrov D, Milchev A, Binder K (2007) Capillary rise in nanopores: molecular dynamics evidence for the Lucas-Washburn equation. Phys Rev Lett 99(5):054501

49. Gruener S, Hofmann T, Wallacher D, Kityk AV, Huber P (2009) Capillary rise of water in hydrophilic nanopores. Phys Rev E 79(6):067301
50. Gelb LD, Hopkins AC (2002) Dynamics of the capillary rise in nanocylinders. Nano Lett 2(11):1281–1285
51. Huber P (2015) Soft matter in hard confinement: phase transition thermodynamics, structure, texture, diffusion and flow in nanoporous media. J Phys: Condensed Matter 27(10):103102
52. Masoodi R, Pillai KM (2012) Wicking in porous materials: traditional and modern modeling approaches. CRC Press, United Kingdom
53. Lin M, Abeles B, Huang J, Stasiewski H, Zhang Q (1992) Viscous flow and diffusion of liquids in microporous glasses. Phys Rev B 46(17):10701
54. Huber P, Grüner S, Schäfer C, Knorr K, Kityk A (2007) Rheology of liquids in nanopores: a study on the capillary rise of water, n-hexadecane and n-tetracosane in mesoporous silica. Eur Phys J Special Topics 141(1):101–105
55. Wang X, Xiao S, Zhang Z, He J (2017) Effect of nanoparticles on spontaneous imbibition of water into ultraconfined reservoir capillary by molecular dynamics simulation. Energies 10(4):506
56. Jiang X, Mishra N, Turner JN, Spencer MG (2008) Diffusivity of sub-1,000 da molecules in 40 nm silicon-based alumina pores. Microfluid Nanofluid 5(5):695–701
57. Kaerger J, Ruthven DM (2016) Diffusion in nanoporous materials: fundamental principles, insights and challenges. New J Chem 40(5):4027–48
58. Dubin SB, Clark NA, Benedek GB (1971) Measurement of the rotational diffusion coefficient of lysozyme by depolarized light scattering: configuration of lysozyme in solution. J Chem Phys 54(12):5158–64
59. Uchiyama S, Arisaka F, Stafford WF, Laue T (2016) Analytical ultracentrifugation. Springer, Germany
60. Javidpour L, Tabar MRR, Sahimi M (2009) Molecular simulation of protein dynamics in nanopores. ii. diffusion. J Chem Phys 130(8):02–613
61. Bruno G, Di Trani N, Hood RL, Zabre E, Filgueira CS, Canavese G, Jain P, Smith Z, Demarchi D, Hosali S, et al (2018) Unexpected behaviors in molecular transport through size-controlled nanochannels down to the ultra-nanoscale. Nature Commun 9(1):1682
62. Amato F, Cosentino C, Pricl S, Ferrone M, Fermeglia M, Cheng MM-C, Walczak R, Ferrari M (2006) Multiscale modeling of protein transport in silicon membrane nanochannels. Part 2, from molecular parameters to a predictive continuum diffusion model. Biomed Microdev 8(4):291–298
63. Missirlis D, Kawamura R, Tirelli N, Hubbell JA (2006) Doxorubicin encapsulation and diffusional release from stable, polymeric, hydrogel nanoparticles. Eur J Pharmaceu Sci 29(2):120–129
64. Lebold T, Jung C, Michaelis J, Brauchle C (2009) Nanostructured silica materials as drug-delivery systems for doxorubicin: single molecule and cellular studies. Nano Lett 9(8):2877–2883
65. Minati L, Antonini V, Dalla Serra M, Speranza G, Enrichi F, Riello P (2013) pH-activated doxorubicin release from polyelectrolyte complex layer coated mesoporous silica nanoparticles. Micropor Mesopor Mater 180:86–91
66. Eikenberry S (2009) A tumor cord model for doxorubicin delivery and dose optimization in solid tumors. Theoret Biol Med Model 6(1):16
67. Korneva G, Ye H, Gogotsi Y, Halverson D, Friedman G, Bradley J-C, Kornev KG (2005) Carbon nanotubes loaded with magnetic particles. Nano Lett 5(5):879–884
68. Kim BM, Qian S, Bau HH (2005) Filling carbon nanotubes with particles. Nano Lett 5(5):873–878

Publisher's Note

Springer Nature remains neutral with regard to jurisdictional claims in published maps and institutional affiliations.

Submit your manuscript to a SpringerOpen journal and benefit from:

- ► Convenient online submission
- ► Rigorous peer review
- ► Open access: articles freely available online
- ► High visibility within the field
- ► Retaining the copyright to your article

Submit your next manuscript at ► springeropen.com